nature astronomy

SUPPLEMENTARY INFORMATION
https://doi.org/10.1038/s41550-019-0731-1

In the format provided by the authors and unedited.

Properties of rubble-pile asteroid (101955) Bennu from OSIRIS-REx imaging and thermal analysis

D. N. DellaGiustina[1,26*], J. P. Emery[2,26*], D. R. Golish[1], B. Rozitis[3], C. A. Bennett[1], K. N. Burke[1], R.-L. Ballouz[1], K. J. Becker[1], P. R. Christensen[4], C. Y. Drouet d'Aubigny[1], V. E. Hamilton[5], D. C. Reuter[6], B. Rizk[1], A. A. Simon[6], E. Asphaug[1], J. L. Bandfield[7], O. S. Barnouin[8], M. A. Barucci[9], E. B. Bierhaus[10], R. P. Binzel[11], W. F. Bottke[5], N. E. Bowles[12], H. Campins[13], B. C. Clark[7], B. E. Clark[14], H. C. Connolly Jr.[15], M. G. Daly[16], J. de Leon[17], M. Delbo'[18], J. D. P. Deshapriya[9], C. M. Elder[19], S. Fornasier[9], C. W. Hergenrother[1], E. S. Howell[1], E. R. Jawin[20], H. H. Kaplan[5], T. R. Kareta[1], L. Le Corre[21], J.-Y. Li[21], J. Licandro[17], L. F. Lim[6], P. Michel[18], J. Molaro[21], M. C. Nolan[1], M. Pajola[22], M. Popescu[17], J. L. Rizos Garcia[17], A. Ryan[18], S. R. Schwartz[1], N. Shultz[1], M. A. Siegler[21], P. H. Smith[1], E. Tatsumi[23], C. A. Thomas[24], K. J. Walsh[5], C. W. V. Wolner[1], X.-D. Zou[21], D. S. Lauretta[1] and The OSIRIS-REx Team[25]

[1]Lunar and Planetary Laboratory, University of Arizona, Tucson, AZ, USA. [2]Department of Earth and Planetary Sciences, University of Tennessee, Knoxville, TN, USA. [3]School of Physical Sciences, The Open University, Milton Keynes, UK. [4]School of Earth and Space Exploration, Arizona State University, Tempe, AZ, USA. [5]Southwest Research Institute, Boulder, CO, USA. [6]NASA Goddard Space Flight Center, Greenbelt, MD, USA. [7]Space Science Institute, Boulder, CO, USA. [8]The Johns Hopkins University Applied Physics Laboratory, Laurel, MD, USA. [9]LESIA, Observatoire de Paris, Université PSL, CNRS, Sorbonne Université, Univ. Paris Diderot, Sorbonne Paris Cité, Meudon, France. [10]Lockheed Martin Space, Littleton, CO, USA. [11]Department of Earth, Atmospheric, and Planetary Sciences, Massachusetts Institute of Technology, Cambridge, MA, USA. [12]Atmospheric, Oceanic and Planetary Physics, University of Oxford, Oxford, UK. [13]Department of Physics, University of Central Florida, Orlando, FL, USA. [14]Department of Physics and Astronomy, Ithaca College, Ithaca, NY, USA. [15]Department of Geology, Rowan University, Glassboro, NJ, USA. [16]The Centre for Research in Earth and Space Science, York University, Toronto, Ontario, Canada. [17]Instituto de Astrofísica de Canarias and Departamento de Astrofísica, Universidad de La Laguna, Tenerife, Spain. [18]Université Côte d'Azur, Observatoire de la Côte d'Azur, CNRS, Laboratoire Lagrange, Nice, France. [19]Jet Propulsion Laboratory, California Institute of Technology, Pasadena, CA, USA. [20]Smithsonian Institution National Museum of Natural History, Washington, DC, USA. [21]Planetary Science Institute, Tucson, AZ, USA. [22]Istituto Nazionale di Astrofisica, Astronomical Observatory of Padova, Padova, Italy. [23]Department of Earth and Planetary Science, The University of Tokyo, Tokyo, Japan. [24]Department of Physics and Astronomy, Northern Arizona University, Flagstaff, AZ, USA. [25]A full list of authors and their affiliations appears at the end of the paper. [26]These authors contributed equally: D. N. DellaGiustina, J. P. Emery. *e-mail: danidg@lpl.arizona.edu; jemery2@utk.edu

Supplementary Materials

Motivation for thermal observations and analysis. Thermal analysis of Bennu is an important objective of the OSIRIS-REx mission. Global and local determination of thermophysical properties of the surface provides temperature predictions for spacecraft safety constraints (the highest surface temperatures pose a potential risk of overheating the spacecraft during sampling), informs the determination of the regolith particle size for sampleability considerations, and enables assessment of mineral and volatile thermal stability for considerations of the relative scientific value of different potential sample sites. Testing and refining the theory of the Yarkovsky effect is also a primary objective of the mission.

With these objectives in mind, we carefully planned a large number of thermal observations during the ~1.5 years of proximity operations before sampling the surface. The Approach-phase observations described here enable direct comparisons to previous Spitzer Space Telescope observations of Bennu and provide the first direct test of the Yarkovsky effect[23]. Data from the Preliminary Survey mission phase in December 2018 provided the first disk-resolved thermal data of Bennu.

Reanalysis of Spitzer space telescope observations. We began the thermal study with a reanalysis of previous thermal observations of Bennu from the Spitzer Space Telescope[12] using the updated shape and spin information from OSIRIS-REx. The Spitzer data consist of 11 point thermal lightcurves at six different wavelengths: 3.6, 4.5, 5.8, 8.0, 16, and 22 µm. The Spitzer observations occurred when Bennu was 1.124–1.143 AU from the Sun, 0.506–0.533 AU from Spitzer, and at phase angles of 61.7–63.5°. Using the shape model derived from radar observations[20], Emery et al. [12] reported a thermal inertia of 310 ± 70 J m^{-2} K^{-1} $s^{-1/2}$, with no rotational variations greater than the reported uncertainty. Our updated analysis with the OSIRIS-REx shape model provides a better fit to the Spitzer data, as illustrated in Supplementary Figure 1 for the 8-µm Spitzer lightcurve. The resulting thermal inertia of 370 ± 20 J m^{-2} K^{-1} $s^{-1/2}$ is within the uncertainties of the previously reported value. We find a fairly rough surface, characterized by RMS surface slopes of 37 ± 2° (a fraction 0.58 ± 0.06 of the surface covered in hemispherical model craters). The new analysis places tighter constraints on rotational variations of thermal inertia (at the global scale) at the level of the new, smaller uncertainties.

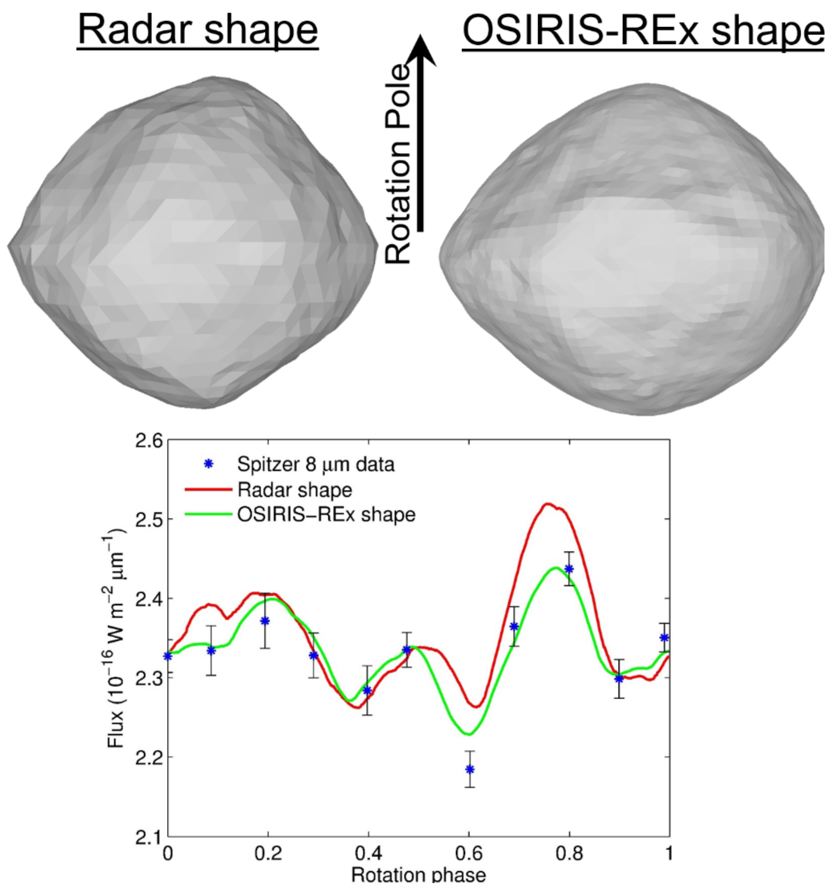

Supplementary Figure 1. Reanalysis of Spitzer data with OSIRIS-REx shape. The shapes of Bennu derived from radar observations[20] and from stereophotoclinometry applied to images of Bennu from OSIRIS-REx are compared at the top of the image. The shape derived from OSIRIS-REx data is slightly more oblate than the radar shape model. The bottom plot shows thermal fluxes of Bennu at 8 µm measured by the Spitzer space telescope (blue points) along with the best fit model thermal lightcurve using the radar shape (red curve) and the OSIRIS-REx shape model (green curve). The OSIRIS-REx shape model produces a significantly improved fit to the Spitzer measurements.

Thermal analysis of OTES and OVIRS approach phase observations. We focused our analysis of the OTES approach-phase data on fitting thermal light curves within individual spectral channels. Because OTES is a Fourier transform interferometer, observations of a target that does not fill and is not centered in the field of view are particularly difficult to properly calibrate. As a result, the absolute flux and relative spectral response for these disk-integrated observations are not well calibrated. OTES was designed and calibrated for disk-resolved observations, and is working very well to design specifications; this complication does not affect observations when Bennu fills the FOV (e.g., the preliminary survey phase observations in December 2018). For the analysis of the disk-integrated data presented here, we therefore focus on the relative time-series data within individual spectral channels. At the low phase angle of the OTES observations (~5°), the relative thermal lightcurves are strongly controlled by the shape and surface roughness; thermal inertia has a very weak effect. As illustrated in

Supplementary Figure 2a, a high surface roughness of ~43^o is required to fit the OTES relative thermal lightcurves.

The thermal radiance from OVIRS data provides strong new constraints on both thermal inertia and roughness of Bennu. Using the OSIRIS-REx-derived shape model and rotation state described in Methods, we are able to accurately reproduce the measured OVIRS thermal radiance, as illustrated in Supplementary Figure 2b. Fitting the OVIRS thermal radiance light curves and spectra in the 3.5 to 4.0 µm, we find a thermal inertia of 350 ± 20 J m^{-2} K^{-2} $s^{-1/2}$ and surface roughness characterized by RMS slope of 43 ± 1^o (0.77 ± 0.04 coverage of hemispherical model craters), in agreement with analysis of the Spitzer data and the OTES data.

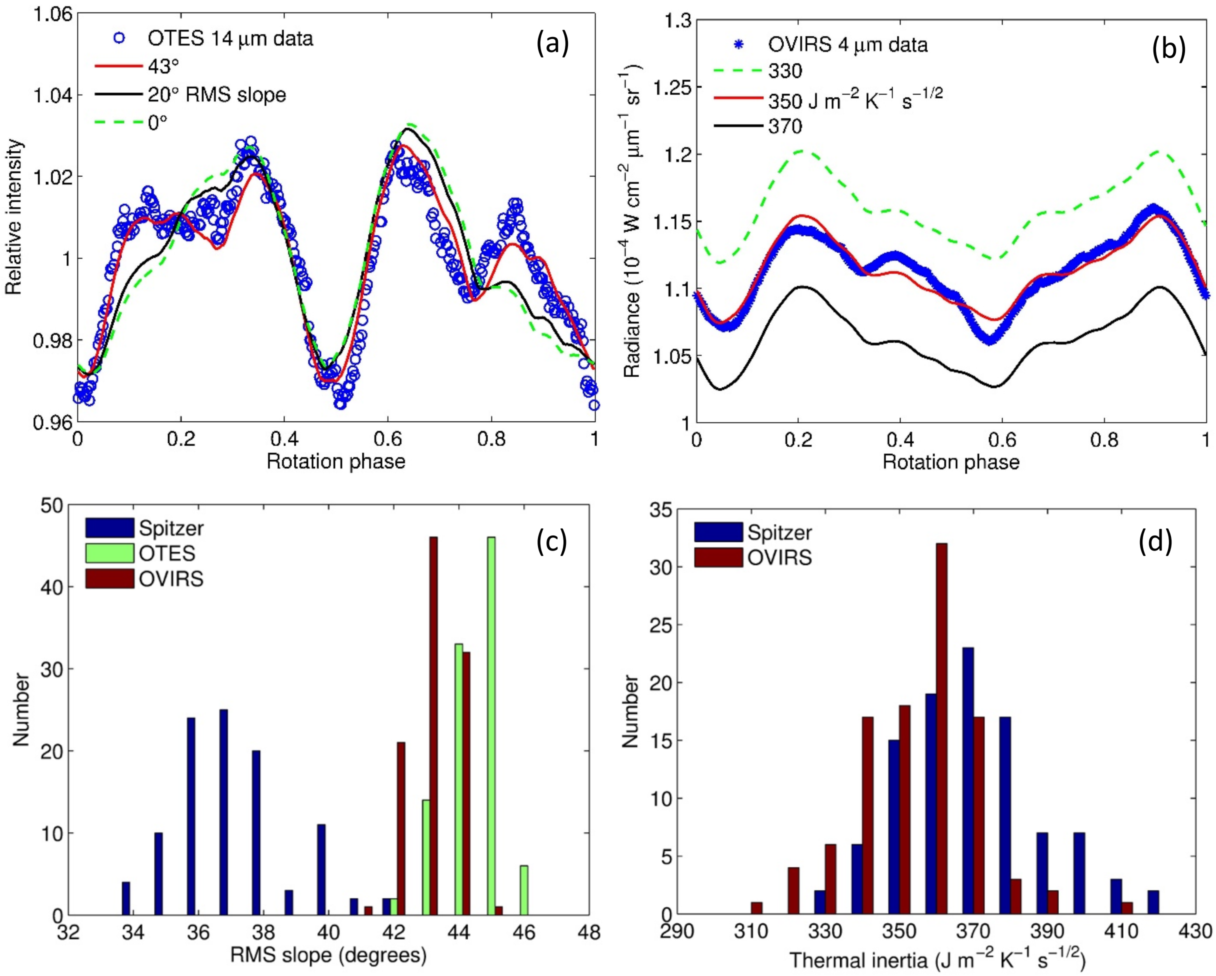

Supplementary Figure 2. a, Thermal model fits to the relative thermal light curve measured by OTES at 14 µm. The OTES data (blue circles) are normalized to the mean signal in this channel and binned to 1° rotational phase. The curves show model fits with different surface roughness for a thermal inertia of 350 J m^{-2} K^{-1} s$^{-1/2}$. A rough surface is required to fit the OTES light curve. Other wavelength channels give similar results. ***b,*** Thermal model fits to the thermal light curve measured by OVIRS at 4 µm. The data are properly calibrated in radiance units in this case. The thermal radiance has been isolated as described in the Methods. The curves show model fits with different thermal inertias for a surface roughness of 43° RMS slope, illustrating the strong constraint on thermal inertia provided by the OVIRS data. ***c,*** Histograms of roughness solutions from the Monte Carlo bootstrap uncertainty analysis described in the Methods section for each of the data sets analyzed in this work. ***d,*** Histograms of the thermal inertia solutions from the Monte Carlo bootstrap analysis.

Thermal model deviates slightly from the OVIRS data at some rotational phases. Near 0.4 rotational phase, for example, the largest boulder rotates into view on the limb of Bennu. This boulder has a fairly flat face and therefore receives direct sunlight and heats up quickly when it rotates into sunlight. Based on its size measured in images, we estimate that the thermal radiance from this large boulder is consistent with the level of departure of the model from the data. However, the boulder, particularly its flat face, is not well represented in the global shape model. We therefore conclude that the deviations between the OVIRS data and thermal model are mostly due to remaining imperfections (such as poorly represented boulders) in the shape model. Nevertheless, ascribing those deviations to thermal inertia variations provides an upper limit to the amount of thermal inertia variation with rotation. Allowing thermal inertia to vary with rotation to ensure a perfect fit to the 4-µm lightcurve suggests variations of < 10 J m^{-2} K^{-1} $s^{-1/2}$ over a full rotational phase.

Global boulder counts

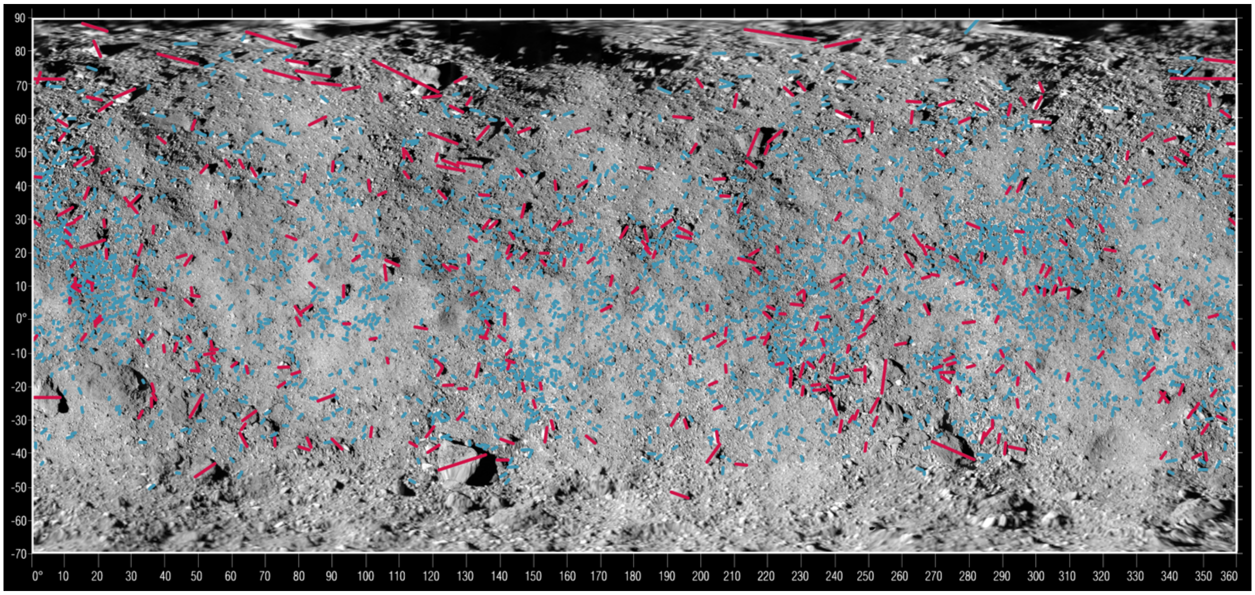

Supplementary Figure 3. The global mosaic of Bennu with an overlay of the shapefile generated from the boulder counts that cover ~80% of the surface of Bennu. These data were used in the cumulative size-frequency distributions presented in this work. Pink lines correspond to the counts that are greater or equal to the completeness limit of (~8 meters) and the blue lines indicate the counts that are below the completeness limit. The geometric information for the counts was calculated using shape model v13, using unprojected L2 OCAMS images (see methods). Counts were performed on unprojected PolyCam image taken on 1 December 2018 with pixel scales between 0.743 and 3.866 m/pixel. There are few to no counts close to the South Pole because the imaging campaign on 1 December did not provide adequate coverage of that area. This global mosaic is created by combining images from 1 December with MapCam images from 16 December 2018 with pixel scales from 0.831 to 1.625 m/pixel.

Cumulative size-frequency distribution of Bennu and other small bodies

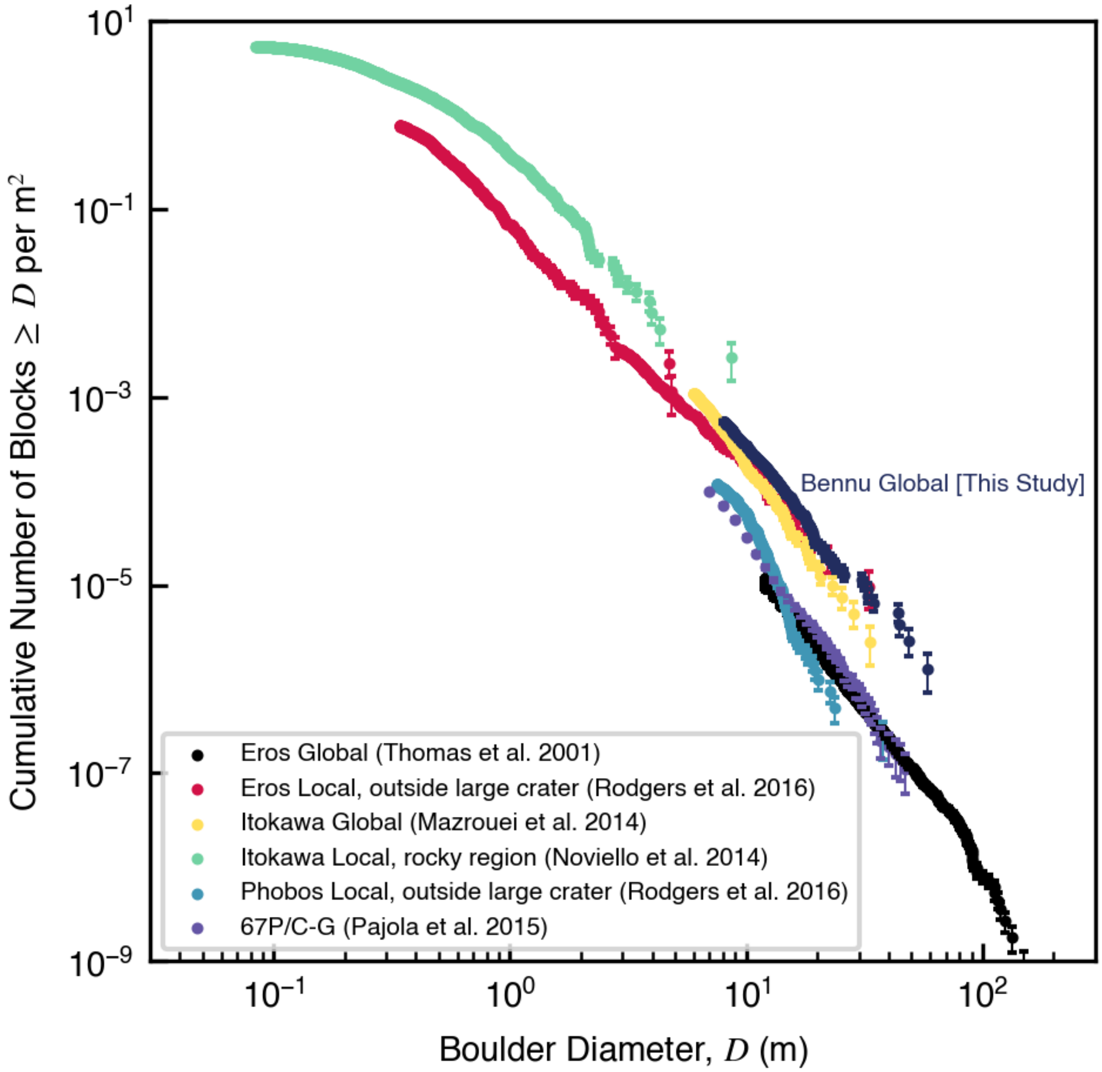

Supplementary Figure 4. The global unbinned cumulative size-frequency distribution (CSFD) of boulders on Bennu compared to several small Solar System bodies [30]. This shows that Bennu's CSFD is within the range observed on other small bodies.

Crater mass ejecta vs. size compared to Bennu's largest boulder and crater

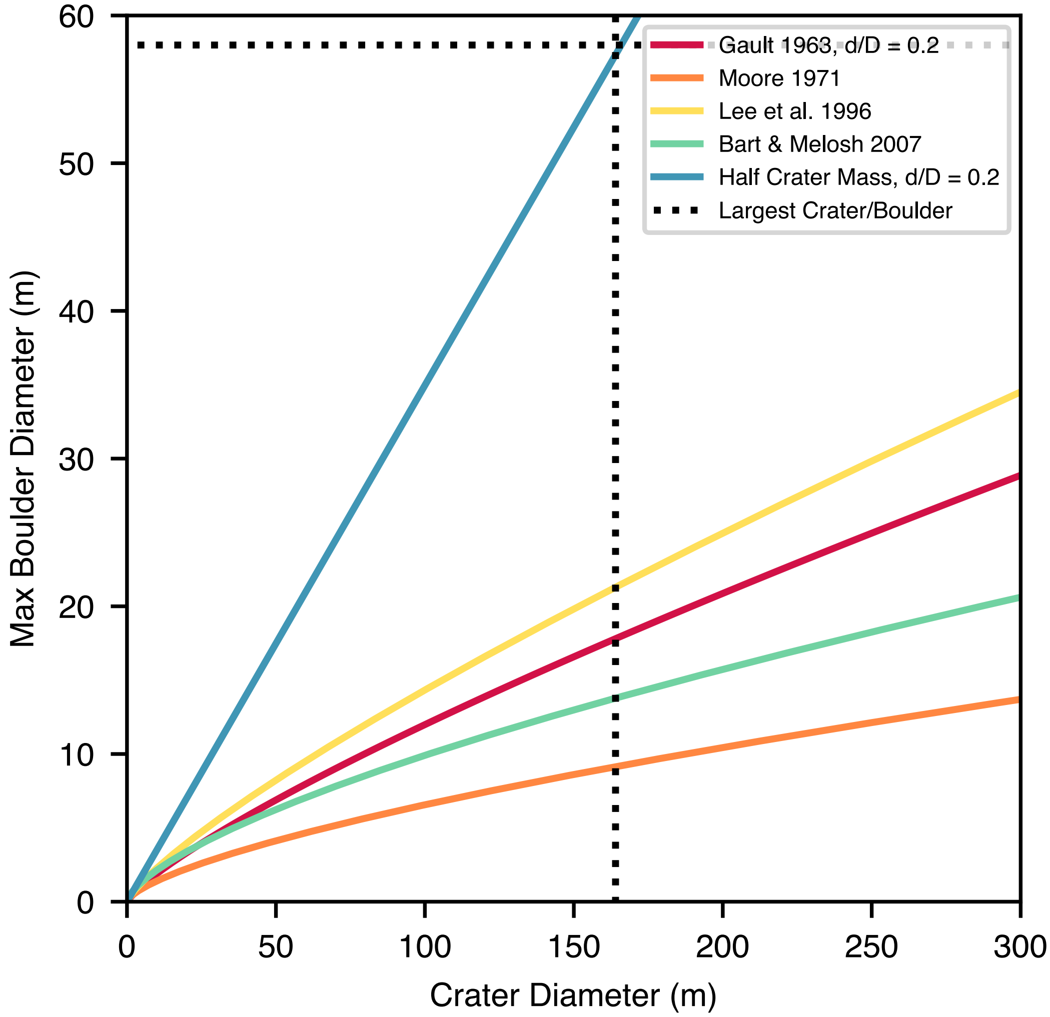

Supplementary Figure 5. The relationship between the mass distribution of crater ejecta and crater size according to several classic scaling law models (shown below). These models encompass analysis of the boulder size-frequency distribution related to impact craters on Earth [67], the Moon [68, 69], and the asteroid (243) Ida [24]. While boulder production through impacts on a rubble-pile asteroid may differ from these larger bodies, it is yet unclear how it scales across gravity and composition; nevertheless, we expect that the fundamental nature of boulder production through impacts to be similar. As a demonstration of the fundamental change in our understanding required to explain crater-related production of the largest boulders on Bennu, we show an unphysical scaling relationship that results in 50% of the crater ejecta being expelled as a single block is necessary to link the existence of the largest boulder (58 ± 6 m) to the largest crater (164 m) on Bennu. We assume conservative d/D of 0.2, compared to the 0.13±0.04 value reported by [3]. Therefore, based on our current understanding of boulder production through impact cratering, we conclude that the largest boulders on Bennu (> 20 m) are likely primordial.

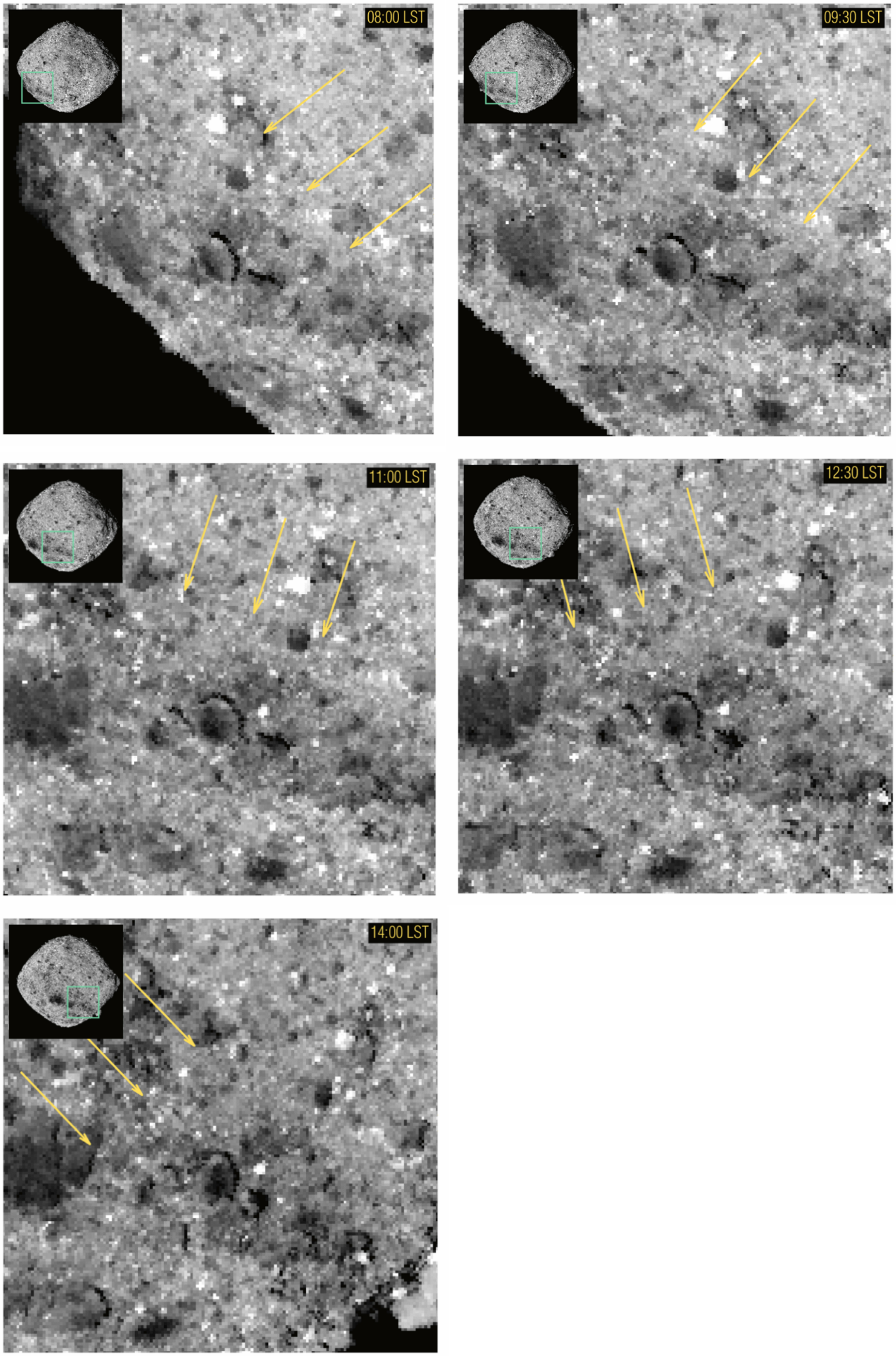
08:00 LST
09:30 LST
11:00 LST
12:30 LST
14:00 LST

Supplementary Figure 6. A series of images taken on 25 November 2018, at a phase angle of ~4^{o}, which highlights the same region shown in Figure 5 of the main text. Yellow arrows indicate the direction of sunlight; the time in the upper right corner is the Local Solar Time at the central boulder in the image; the inset indicates the region of interest on Bennu. All images have been stretched identically. Images show a consistent unit of dark diffuse material mantling the central boulder area. The consistent appearance of the dark material throughout a Bennu day indicates that these units represent albedo differences and are not shadowing due to terrain.

Surface roughness

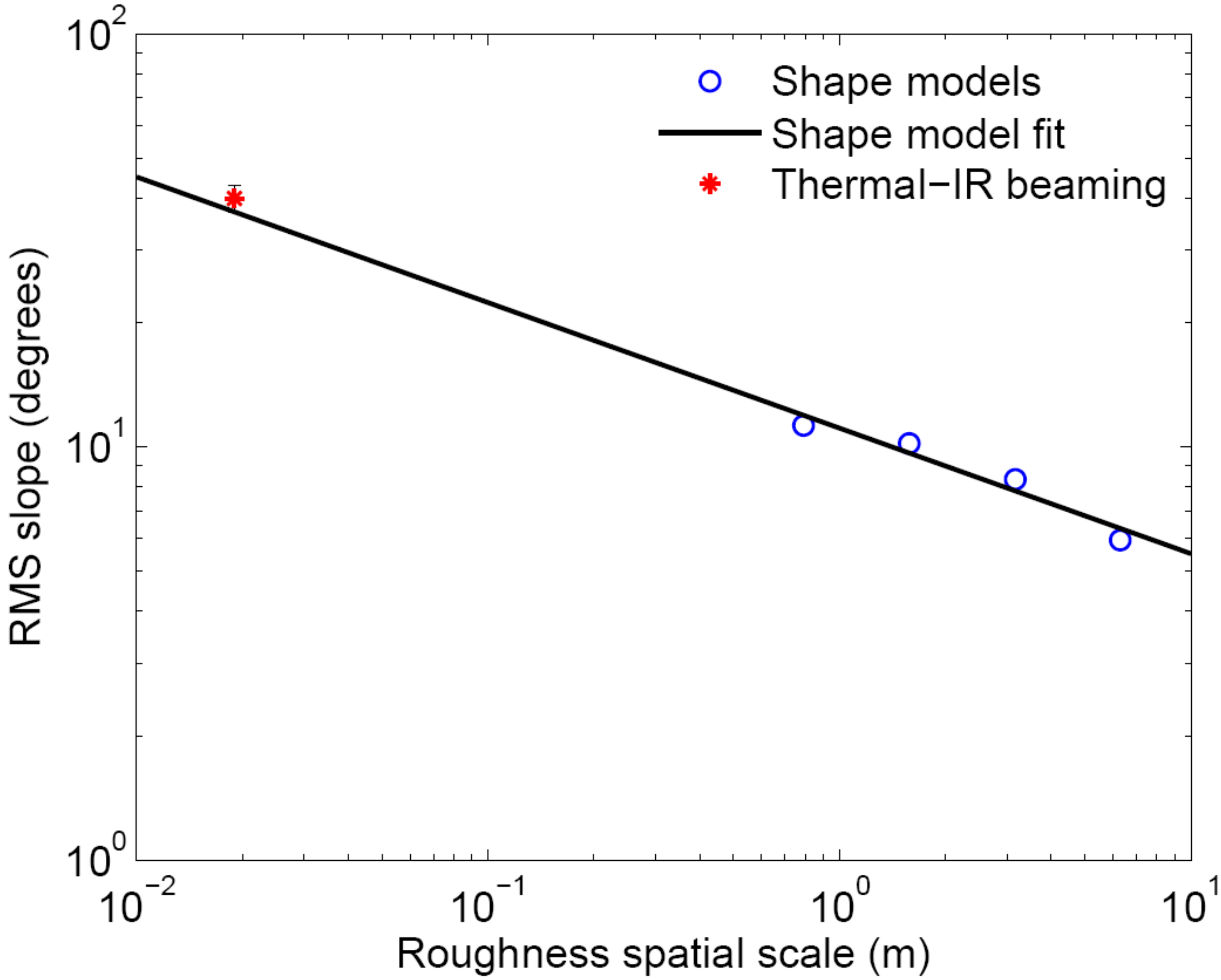

Supplementary Figure 7. Comparison of the roughness required to fit the observed thermal-infrared beaming from Bennu to roughness computed at the scales of different versions of the OSIRIS-REx shape model. Blue circles are roughness computed at scales of 6.3 m, 3.2 m, 1.6 m, and 0.8 m relative to the 12.6 m resolution shape model used for thermal analysis. The black line is a power-law fit to the blue circles. The red asterisk is the roughness determined from fitting the thermal data. It is placed at the roughness scale where the error bar crosses the extrapolation of the fit to the shape model roughness – about 2 cm. These results suggest that the thermal infrared beaming is most sensitive to the smaller end of the spatial scale (i.e., close to the thermal skin depth), and that Bennu is much rougher at these scales than at larger spatial scales. See [43] for more discussion of thermal infrared roughness.

OVIRS thermal radiance

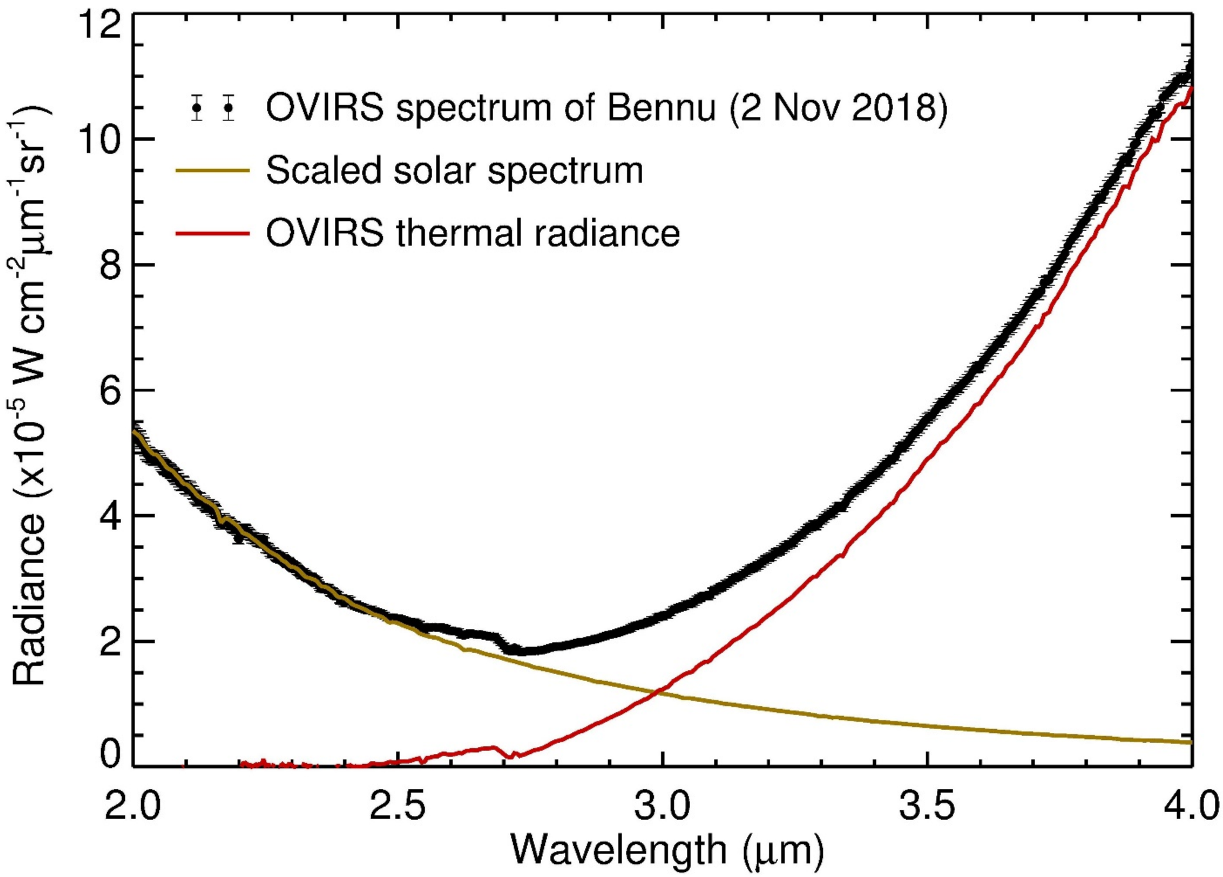

Supplementary Figure 8. Illustration of the isolation of thermal radiance in OVIRS data. The solar spectrum (gold line) was scaled to the observed OVIRS radiance (black points) at ~2.1 µm, where the data are dominated by reflected sunlight. The scaled solar spectrum represents the continuum reflected radiance from Bennu, assuming a flat spectral slope. This estimate of reflected radiance is then subtracted from the observed total radiance. The result is the thermal radiance (red line), which is used in the thermal analysis.